Selective Probing of Thin Film Interfaces Using Internal Reflection Sum-Frequency Spectroscopy

Md. Shafiul Azam, Canyu Cai, and Dennis K. Hore

August 2019

Selective Probing of Thin Film Interfaces Using Internal Reflection Sum-Frequency Spectroscopy

Md. Shafiul Azam,[†] Canyu Cai,[†] and Dennis K. Hore[*,‡]

†*Department of Chemistry, University of Victoria, Victoria, Canada, V8W 3V6*

‡*Department of Chemistry, University of Victoria, Victoria, Canada, V8W 3V6; Department of Computer Science, University of Victoria, Victoria, British Columbia, V8W 3P6, Canada*

E-mail: dkhore@uvic.ca

Abstract

The study of interfacial properties of thin films such as polymers is an important area of surface science. The application of visible-infrared sum-frequency generation spectroscopy to such systems requires a careful interpretation of the results, as the electric field magnitude and phase at each interface must be determined in a manner that takes thin film interference effects into account. Several schemes have been proposed for handling the local field corrections, and these methods all have their origins in linear optics. We first provide an extensive discussion of the cases in which the film is sufficiently thick that multiple beam interference can be ignored, or sufficiently thin in which the relevant expressions collapse to simple forms. Then we illustrate a straightforward method that has a concise analytic solution in the case of a single thin film that exhibits interference effects. We demonstrate a visualization technique that allows the experimental geometry to be tuned to select the interface of interest, and rapidly switch between the interfaces when the film thickness is chosen to accommodate this.

Introduction

Over the past three decades, visible-infrared sum-frequency generation (SFG) spectroscopy has developed into a feature rich structural probe of surfaces and buried interfaces.[1–3] Its surface specificity stems from the fact that, under the electric dipole approximation, the second-order electric susceptibility $\chi^{(2)}$ is non-zero only in regions that lack an inversion centre, i.e. in regions over which there is no point such that $(x, y, z) \rightarrow (-x, -y, -z)$.[4] Niche applications are therefore found at the interface between two centrosymmetric media, such as air, bulk liquids, and isotropic solids including polymers.[5,6] In such cases, the intensity of the i-polarized SFG signal is related to the intensity of the incident j-polarized visible and k-polarized infrared beams through

$$I_{i,\mathrm{SFG}} = \frac{8\pi^3 \omega_{\mathrm{SFG}}^2 \sec^2\theta_{\mathrm{SFG}}}{c^3 n_{\mathrm{SFG}} n_{\mathrm{vis}} n_{\mathrm{IR}}} |\chi^{(2)}_{ijk,\mathrm{eff}}|^2 I_{j,\mathrm{vis}} I_{k,\mathrm{IR}}. \tag{1}$$

Elements of the effective second-order susceptibility are related to the actual second-order susceptibility through the relation

$$\chi^{(2)}_{ijk,\mathrm{eff}} = L_{ii,\mathrm{SFG}} : \chi^{(2)}_{ijk} \cdot L_{jj,\mathrm{vis}} \cdot L_{kk,\mathrm{IR}} \tag{2}$$

where L_{jj} and L_{kk} relate the incoming visible and infrared electric fields to the corresponding fields at the interface where $\chi^{(2)} \neq 0$, and L_{ii} is the equivalent local field correction for the SFG field generated at the interface to be propagated out of the material.

In addition to considering a single interface between two semi-infinite media, there is considerable interest in applying SFG spectroscopy to stratified interfaces consisting of one or more layers. Among such samples, one of the most commonly-encountered systems is a polymer film spin-coated onto a substrate, with a polymer thickness in the range of tens of nanometers up to a few hundred nanometers. As facile analysis of the SFG signal to extract quantitative structural information relies on smooth surfaces that can generate specular reflection, the film thickness must generally be kept below 1000 nm. However, the experimental convenience of spin coating films with this range of

thicknesses presents an analysis challenge, as multiple beam interference necessarily occurs for the SFG, visible, and infrared beams, as is well known in the linear optics community.

There have been many schemes proposed for dealing with the effects of multiple beam interference in SFG spectroscopy[7–18] and these have been successfully applied to aid in the interpretation of many systems.[19–24] Approaches generally fall into three categories: those based on the Airy formulas,[10–14,16,21–25] Abèles formalism,[26] or a transfer matrix approach.[7–9,15,17,18,20] These techniques are all capable of generating the same results, but are ideally suited to specific systems. For example, the geometric converging infinite series in the Airy approach is cumbersome to expand when there are more than a few phases. Matrix techniques have the advantage of being easily extended to systems with an arbitrary number of layers, but result in solutions that are sometimes not obvious in the case where there is only one film present. In this account, we first discuss some practical considerations from an experimental perspective, highlighting cases where the phases are either sufficiently thin or sufficiently thick so as to not require any interference calculations. We then present a formalism based on Abèles method that can be described succinctly when applied to a single thin film. Finally, we present a visualization method that is particularly useful when the objective is not to include the effects of multiple sources of SFG from $\chi^{(2)}$ terms present at different interfaces, but to aid in the selection of experimental geometries that suppress signals from the undesired interface. We provide a practical scheme by which these methods can be applied, and demonstrate results with a polydimethylsiloxane film exposed to air, water, and a perfluorinated liquid.

Background

We consider a film sandwiched between two semi-infinite bulk media. One phase is the substrate on which the film film is coated. The other can be either air, another polymer, aqueous solution or another liquid. The most straightforward case to consider is one where the incident medium (medium 1) is not absorbing for any of the frequencies of interest. Strictly speaking, medium 1

does not have to be perfectly transparent, but the analysis and the points we wish to ultimately make are greatly simplified under this assumption. We are then faced with the situation where, we cannot rule out *a priori* whether $\chi^{(2)} \neq 0$ at the substrate–film interface, the film–ambient/environmental interface, or both. Before getting into the multiple beam interference problem, it is useful to consider if there are any simple experimental situations where the measured signal can safely be assumed to originate from only one of two surfaces.

Thick films

With reference to Fig. 1, the first question is whether the film thickness d could be large enough so that beams may be selectively overlapped at one of the two interfaces. This is not possible as, for typical refractive indices and beam angles, if the visible and infrared with diameters of 200 μm each were 100% overlapped at the interface between media 1 and 2, simple trigonometric relationships indicate that 0% overlap ($\ell_2 > 200$ μm in Fig. 1) at the interface between media 2 and 3 would occur only for $d > 2$ mm. Likewise, if the pulses had a duration of 20 ps, the temporal overlap would be lost only for $d > 4$ mm. In other words, for films with $d < 1000$ nm, the beams are essentially overlapped perfectly in space and time at both interfaces. Another possibility is to set up a pinhole so that dashed blue line in the reflected SFG in Fig. 1 is blocked. But for ℓ_1 to be greater than the diameter of the beams, we require $d > 5$ mm.

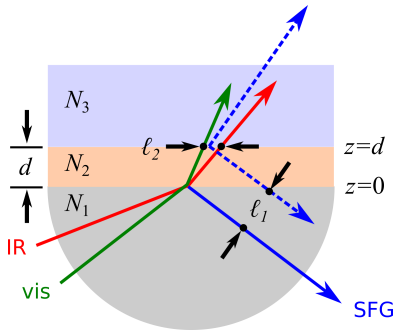

Figure 1: A film of refractive index N_2 and thickness d, situated between two semi-infinite media with indices N_1 and N_3. SFG reflected from the top surface is spatially separated from SFG reflected from the bottom surface by a distance ℓ_1. If incoming visible and infrared beams are spatially overlapped at the top surface, the center of the beams are separated by ℓ_2 at the bottom surface.

One then contemplates how thick the film would have to be so that one of the incident beams is sufficiently attenuated by absorption in passing through before reaching the second interface. It is often discussed that, in the C–H stretching region of the mid-infrared such a situation may be readily realized with spin-coated samples. We consider the most intense band in this region for polydimethylsiloxane (PDMS), the 2910 cm^{-1} methyl symmetric stretch with imaginary part of the refractive index $\kappa = 0.05$. Even with such a large value of κ, this translates to 50% of the IR intensity still present after a path length of 4 μm. With an IR beam incident at 70°, this still requires $d > 1.5$ μm. More concerning is that the mode with the next strongest oscillator strength, the methyl antisymmetric stretch at 2960 cm^{-1} has a value of κ that is approximately 10 times smaller, so one would require $d > 15$ μm to lose 50% of the IR intensity. The ramifications of this quick analysis is not only that sufficient IR intensity is present in the C–H stretching region of organic thin films to simultaneously excite contributions from $\chi^{(2)}$ at both interfaces, but that one may expect severe spectral distortions on account of the varying degrees of IR attenuation.

Another possibility concerns the ratio between the transmitted (upwards pointing dashed blue line in Fig. 1) and reflected (solid blue line) SFG fields in relation to the contrast between the refractive indices N_1 and N_2. Many polymers are nearly index matched to glass in the visible region ($N_1 \approx N_2$), and are not far off from this condition in the infrared. We will later demonstrate that such index-matching plays no role. Even though this results in practically no visible and infrared reflection at the medium 1–medium 2 boundary, there can still be a substantial amount of reflected SFG if $\chi^{(2)} \neq 0$ there.

One simple solution remains, and that is to have the beams incident from either side, and then exclude contributions from the second interface by virtue of *all* of the above phenomena. In other words, if films could be prepared with d on the order of millimeters, then there is no doubt since no SFG is possible due to IR absorption, and we lack both spatial and temporal overlap. However, it is quite challenging to selectively probe the polymer–air interface using any method preparing thick films, since the surface roughness rapidly increases with solution concentration and is inversely proportional to the spinning speed.[27,28] In such cases, it is better to face the multiple

beam interference challenge, as we will demonstrate that good results may be obtained for thin films with a smooth upper surface.

Layers with molecular dimensions

The last case to consider is one where a monolayer or near monolayer of molecules is deposited onto a substrate. This is also a single-layer (3-phase) system, except that the 'layer' has dimensions on the order of a few nanometers. We maintain the same convention where the incident medium as index N_1, and the environmental side (air or aqueous phase in Fig. 1) has index N_3. Here the ratio of the fields in the molecular layer with respect to the incident p- and s-polarized fields are

$$L_{xx}^{d/2} = \frac{E_x^{z=d/2}}{E_{\mathrm{p}}^{z=-\infty}} = (1 - r_p)\cos\theta \tag{3a}$$

$$L_{yy}^{d/2} = \frac{E_y^{z=d/2}}{E_{\mathrm{s}}^{z=-\infty}} = (1 + r_s) \tag{3b}$$

$$L_{zz}^{d/2} = \frac{E_z^{z=d/2}}{E_{\mathrm{p}}^{z=-\infty}} = (1 + r_p)\sin\theta \left(\frac{N_1}{N'}\right)^2. \tag{3c}$$

and N' is the refractive index of the molecular layer.[2,29] Here r_p and r_s are the standard Fresnel reflection coefficients[30]

$$r_p = \frac{N_3\cos\theta_1 - N_1\cos\theta_3}{N_1\cos\theta_3 + N_3\cos\theta_1} \tag{4a}$$

$$r_s = \frac{N_1\cos\theta_1 - N_3\cos\theta_3}{N_1\cos\theta_1 + N_3\cos\theta_3}. \tag{4b}$$

with care given to the sign convention used in the definition of r_p. We label these values of the fields as those obtained at $z = d/2$ although, for such dimensions, there is no appreciable variation with z within the molecular layer. It is, in general, not straightforward to arrive at a value of N' for several reasons: (1) it is sensitive to the local environment of the molecules, which may be substantially different from what they experience in a bulk phase with index N_2; (2) the interfacial electronic structure is influenced by N_1 and N_3; (3) N' depends on the degree of order within the

molecular layer, and so is anisotropic; in the simplest case $N'_x = N'_y \neq N'_z$. This last point results in a circular argument, since one of the goals of polarized SFG spectroscopy is to provide a quantitative description of the molecular orientation—an account of this anisotropy—through measurement of the non-zero values of the $\chi^{(2)}$ tensor and yet the local field correction factor L_z depends the precise details of the molecular arrangement! Fortunately, there are many cases in which approximations for L_{zz}, including an isotropic assumption, do not severely impact the experimental effort.

Thin films that exhibit interference effects

There have been many methods and formalisms proposed for the calculation of the mean square fields. Some of these have been popularized due to their convenience, especially before computers were widely available. As it is not our intention to provide a comprehensive review or even list the various approaches, we will describe only one method, that is often referred to as the exact, or electrodynamic, treatment as it incorporates the thickness and complex refractive index of each material explicitly. This is the technique originally proposed by Abèles and extended by Hansen,[31] and then Axelsen and Citra.[32] This method treats the general case of light incident from a transparent semi-infinite phase (such as air, $N_1 = n_1$, $\kappa_1 = 0$) with angle θ_1 with respect to the surface normal $\hat{z}$ onto a stratified system. Each layer j of thickness d_j has complex refractive index $N_j = n_j + i\kappa_j$, where $i = \sqrt{-1}$. Finally the beam encounters the last semi-infinite phase with $N_N = n_N + i\kappa_N$. The exact solution may be formulated in a matrix form where each of the layers (from $j = 2$ to $j = N - 1$) is accounted for by a matrix $\mathbf{M}_j$ that relates the tangential components U of the electric, and V of the magnetic parts of the electromagnetic field at the first surface ($z = z_1 = 0$) to the last surface ($z = z_N$)

$$\begin{bmatrix} U_1 \\ V_1 \end{bmatrix} = \mathbf{M}_2\mathbf{M}_3\mathbf{M}_4 \cdots \mathbf{M}_{N-1} \begin{bmatrix} U_{N-1} \\ V_{N-1} \end{bmatrix} \tag{5}$$

where

$$\mathbf{M}_j = \begin{bmatrix} \cos\beta_j & -\dfrac{i}{p_j}\sin\beta_j \\ -ip_j\sin\beta_j & \cos\beta_j \end{bmatrix} \tag{6}$$

and $p_j^s = N_j \cos\theta_j$ with θ_j the refracted angle in medium j for s-polarized light (**E** along $\hat{y}$, perpendicular to the plane of incidence), and $p_j^p = p_j^s / N_j^2$ for p-polarized light (components of **E** along $\hat{x}$ and $\hat{z}$, parallel to the plane of incidence. The term accounting for the phase of the fields between the layers is defined as

$$\beta_j = \frac{2\pi d_j p_j}{\lambda}. \tag{7}$$

This matrix **M** is powerful as it directly leads to the transmittance and reflectance spectra. Our objective is to arrive at the electric fields, so we invert **M** to obtain

$$\mathbf{N}_j = \left(\mathbf{M}_j\right)^{-1} = \begin{bmatrix} \cos\beta_j & \dfrac{i}{p_j}\sin\beta_j \\ ip_j \sin\beta_j & \cos\beta_j \end{bmatrix} \tag{8}$$

with

$$\beta_k = \frac{2\pi}{\lambda} p_k (z - z_{k-1})$$

where z_{k-1} is the thickness of phase $k-1$. These **N** matrices may be used to obtain U, V, and W at any location z in material k according to

$$\begin{bmatrix} U_k(z) \\ V_k(z) \end{bmatrix} = N_k(z) \prod_{j=k}^{2} N_j \begin{bmatrix} U_{N-1} \\ V_{N-1} \end{bmatrix} \tag{9a}$$

$$W_k(z) = \frac{N_1 \sin(\theta_1)}{N_k^2} U_k(z). \tag{9b}$$

Finally the quantities of interest are obtained via

$$E_x = U_k(z) \tag{10a}$$

$$E_y = V_k(z) \tag{10b}$$

$$E_z = W_k(z). \tag{10c}$$

Readers interested in further details of these expressions can refer to the original work.[31,32] As a result of these steps, explicit formulations of this result (for example, for 2- or 3-phase systems), or approximate equations for $\langle|\mathbf{E}|^2\rangle$, have historically been of interest. Nevertheless, this formalism indicates that, so long as the refractive index N and thickness d are known for each material, $\langle E_x^2\rangle$, $\langle E_y^2\rangle$, $\langle E_z^2\rangle$ may be readily determined.

Experimental

Sample preparation. Thin films of PDMS were prepared on IR-grade fused silica hemicylinder prisms (25 mm × 25 mm flat face, Quartz Plus). The prisms were cleaned in a 500 mL glass beaker containing piranha solution, a 3:1 mixture of sulfuric acid and 30% hydrogen peroxide, for 1 h. *(Note: use caution, piranha solution reacts explosively with organic compounds, should not be mixed with any organic materials.)* They were then transferred into a 500 mL Teflon beaker and copiously rinsed (5 × 300 mL) with 18.2 MΩ·cm deionized water (Milli-Q), then rinsed individually under a stream for 30 s, sonicated in 300 mL water for 2 min, and again rinsed with water (2 × 300 mL). The prisms were then placed in a preheated vacuum oven at 85°C for 1 h prior to PDMS coating. PDMS solutions were prepared using a Sylgard 184 silicone elastomer kit (Dow Corning). The base and curing agent were dissolved in spectral grade $CHCl_3$ (Fisher) to prepare 5% (wt/wt) solutions of each and then mixed in a 10:1 (A/B, wt/wt) ratio to obtain a 5% (wt/wt) solution. The prism was secured in a custom chuck adapted for our spin-coater (Specialty Coating Systems, Inc.). Approximately 300 μL of PDMS solution was placed on the flat face of the hemicylindrical prism and cast at 5000 rpm for 5 min. Finally, the samples were placed in an oven and cured at 85°C for 4 h under vacuum.

Film thickness measurement and selection. For subsequent data treatment, we need to know the precise thickness of the PDMS films. However, the challenge is to determine the thickness in a way that does not destroy or contaminate the films, as it is ideal to characterize them prior to SFG measurements. Also, the measurement should be fast (on the timescale of minutes) to prevent

exposure to the environment that would also result in eventual contamination. Direct profilometry measurements are therefore out, as several scratches would need to be made (that could also damage the prism) and those measurements are time-consuming. Ellipsometry is not possible as there is not sufficient refractive index contrast between the polymer and glass. We have therefore developed an alternate two-step method that overcomes these challenges.

Reference films of PDMS were prepared on glass microscope slides (Fisher Scientific) following the aforementioned procedure, with the concentration within a range of 2.5% to 10.0% to obtain variable thicknesses. The thickness of the spin-coated PDMS on microscopic slides was then measured using stylus profilometer (Bruker Dektak XT). Several scratches were made on the freshly prepared substrate using a razor blade and the film thicknesses were obtained from the respective depth profiles. The average thickness of multiple measurements are plotted as a function of the PDMS concentration used to prepare the film in Fig. 2a. Next, Raman spectra were recorded (Renishaw inVia reflex) after adjusting the sample height to maximize the signal. This procedure works since the depth resolution (ca. 5 μm using a 0.75 NA objective) was much larger than the film thickness. The Raman intensities obtained at 2905 cm^{-1} were then plotted as a function of the thickness measured by the profilometry as shown in Fig. 2b. The correlation between the Raman intensity and the film thickness from this calibration eventually allowed us to determine the thickness of the PDMS film, particularly on the hemicylindrical prisms, simply by knowing the Raman intensity of the 2905 cm^{-1} peak.

Description of the laser system. Full details of the laser system used for SFG spectroscopy have been provided previously.[33] In brief, a wavelength-scanning $\approx$ 20 ps SFG spectrometer (Ekspla, Lithuania) with nominally 4 cm^{-1} bandwidth in the IR has been used with custom stages that enable the sample and detector to be rotated about the same axis, in line with the solid (film)–liquid interface at the flat side of the hemicylindrical prism as shown in Fig. 3. For a given film thickness, this enables the incident beam angles to be set with a precision of $\pm 0.3^\circ$ for the visible beam on account of the +750 mm focal length lens, and $\pm 1.7^\circ$ for the IR beam using a +150 mm lens. This spread of angles was calculated using the collimated diameter of 6 mm for both IR and visible

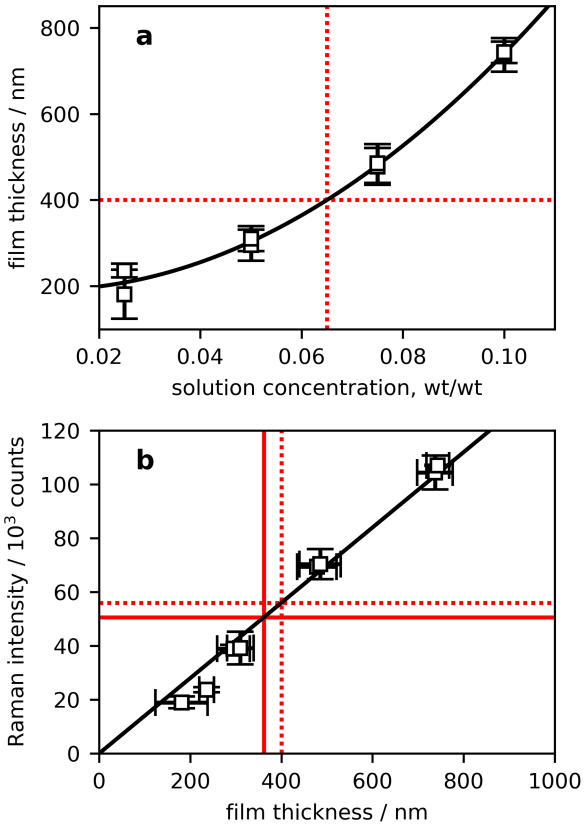

Figure 2: (a) Profilometry measurements of PDMS film thickness for various concentrations of PDMS in $CHCl_3$. (b) Correspondence between Raman scattering intensity of the 2905 cm^{-1} peak and the film thickness.

beams, and the numerical aperture of the individual focusing lenses. Both beams are fixed on the optical table, with the infrared angle of incidence greater by 9.8°. The detector angle was independently set using the known refractive index of the prism.

Results and Discussion

Single-layer thin film systems

The expressions provided in Eq. 10 may be used to solve for the electric field at any point z in a system consisting of an arbitrary number of layers. We now turn to the most commonly-encountered case of a single thin film composition a 3-phase system, for example air–film–substrate in external

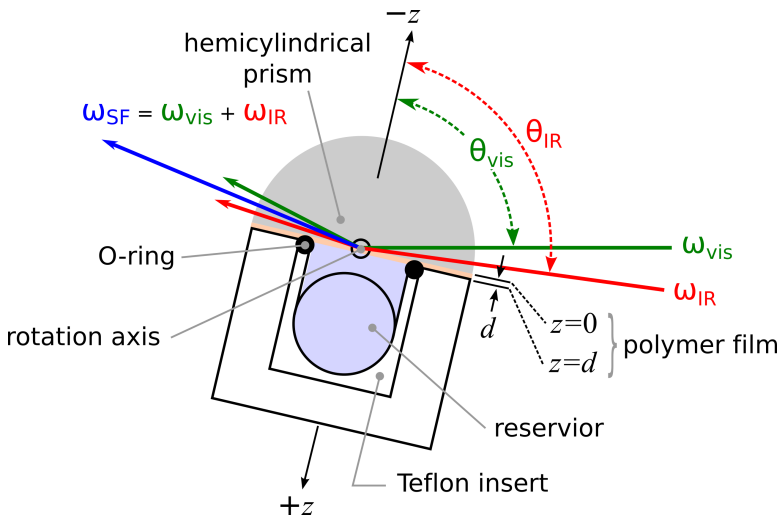

Figure 3: Schematic of the sample cell, illustrating the prism–polymer interface at $z = 0$ and the polymer–air/liquid interface at $z = d$. Fixed beam angles on the table with a common axis of rotation for the sample and detector enable any angle of incidence to be automatically selected while maintaining $\theta_{\mathrm{IR}} - \theta_{\mathrm{vis}} = 9.8°$.

reflection, or substrate–film–aqueous in internal reflection. If we assume that there is no SFG generated in the bulk of any of the three phases, then signal can arise from only the initial film surface (which we refer to as $z = 0$) or the second film surface ($z = d$, where d is the film thickness). In external reflection, $z = 0$ is the air–film interface and $z = d$ is the buried film–substrate interface. In the case of internal reflection, the prism–film interface is at $z = 0$ while the film–air/aqueous interface is at $z = d$.

As the results of the interfacial field calculation are compact, it is worth stating them explicitly. First, the entire system is described by

$$\mathbf{M} \equiv \mathbf{M}_2 = \begin{bmatrix} \cos\beta_2 & -\dfrac{i}{p_2}\sin\beta_2 \\ -ip_2\sin\beta_2 & \cos\beta_2 \end{bmatrix} \tag{11}$$

resulting in the reflection coefficients

$$r = \frac{p_1(M_{11} + p_3M_{12}) - (M_{21} + p_3M_{22})}{p_1(M_{11} + p_3M_{12}) + (M_{21} + p_3M_{22})} \tag{12}$$

with r_s and r_p obtained using the appropriate definitions of p_1, p_2, and p_3 for s- and p-polarization

as noted above. At the first interface the incident visible and infrared beams encounter, we then have the surface fields with respect to the incident fields

$$L_{xx}^{0} = \frac{E_x^{z=0}}{E_{\mathrm{p}}^{z=-\infty}} = (1 - r_p)\cos\theta \tag{13a}$$

$$L_{yy}^{0} = \frac{E_x^{z=0}}{E_{\mathrm{s}}^{z=-\infty}} = 1 + r_s \tag{13b}$$

$$L_{zz}^{0} = \frac{E_x^{z=0}}{E_{\mathrm{p}}^{z=-\infty}} = (1 + r_p)\sin\theta\left(\frac{N_1}{N'}\right)^2. \tag{13c}$$

where N' is again the refractive index of the infinitesimal thin layer of polymer that generates the nonlinear polarization leading to SFG signal. As a first approximation, it is reasonable to consider $N' \approx N_2$, where the polymer surface has the same refractive index as the bulk polymer. However, this does not account for the microscopic components of the local field correction, namely the influence of a semi-infinite distribution of neighbouring molecules, and the anisotropy in the interfacial layer. For this reason a mixing rule, for example $N' \approx \frac{1}{2}(N_1 + N_2)$ may be considered; more sophisticated expressions may be found in the literature.[34,35] Either way, we note that Eq. 13 has the same form as Eq. 3 (ultra thin film), except that r_p and r_s are now derived from a model (Eq. 12) that takes multiple reflections inside the thin film into account.

At the second interface, the local field correction factors are given by

$$L_{xx}^{d} = \frac{E_x^{z=d}}{E_{\mathrm{p}}^{z=-\infty}} = (1 - r_p)\cos\theta\cos\beta_2 + i\frac{N_1\cos\theta_2}{N_2}(1 + r_p)\sin\beta_2 \tag{14a}$$

$$L_{yy}^{d} = \frac{E_y^{z=d}}{E_{\mathrm{s}}^{z=-\infty}} = (1 + r_s)\cos\beta_2 + i\frac{N_1\cos\theta}{N_2\cos\theta_2}(1 - r_s)\sin\beta_2 \tag{14b}$$

$$L_{zz}^{d} = \frac{E_z^{z=d}}{E_{\mathrm{p}}^{z=-\infty}} = \left[\frac{N_1^2}{N_2^2}\sin\theta(1 + r_p)\cos\beta_2 + i\frac{N_1\sin\theta\cos\theta}{N_2\cos\theta_2}(1 - r_p)\sin\beta_2\right]\left(\frac{N_2}{N''}\right)^2 \tag{14c}$$

where N'' is the refractive index of the polymer film in the immediate region of second interface, for example $N'' \approx N_2$ or $N'' \approx \frac{1}{2}(N_2 + N_3)$. Note that r_{p} and r_{s} are again provided by Eq. 12.

Interface selectivity

We now consider the ssp polarization scheme. Using Eq. 13 we plot $(L_y^0)_{\mathrm{SFG}}$, $(L_y^0)_{\mathrm{vis}}$, and $(L_z^0)_{\mathrm{IR}}$ in the left column of Fig. 4. The equivalent results, but for the interface at $z = d$ are plotted in the middle column of Fig. 4. As dispersion and absorptive effects are very important in the calculation of these quantities,[36] we have used frequency-dependent refractive index data for fused silica,[37] PDMS,[38,39] and water.[40] No infrared refractive index data was available for FC40, so we have used $N = 1.29$.[41] This is a reasonable approximation as FC40 has no IR resonances in the frequency range of our interest. We have compared these results to those calculated using Airy formulas, and using the transfer matrix approach[7–9] and found all three methods to be numerically identical. It is important to note that, in the case where both interfaces are SFG-active, the intensity is given by

$$\begin{aligned} I_{\mathrm{ssp}} &\propto \left| L_{yy}^0 L_{yy}^0 L_{zz}^0 \chi_{yyz,0}^{(2)} + L_{yy}^d L_{yy}^d L_{zz}^d \chi_{yyz,d}^{(2)} \right|^2 \\ &\equiv \left| (LLL)_0 \chi_0^{(2)} + (LLL)_d \chi_d^{(2)} \right|^2 \end{aligned} \tag{15}$$

and, even if the L factors are calculated, Eq. 15 can provide predictions only in the case where the magnitude and phase of both $\chi^{(2)}$ values are known. In other words, if only $|\chi_0^{(2)}|$ and $|\chi_d^{(2)}|$ are known (as can be readily determined from a combination of internal and external reflection experiments from sufficiently thick films), the missing phase information prevents Eq. 15 from being applied.

Our approach, however is to arrive at combinations of the incident angles θ and film thickness d so that, when measurement of $\chi_0^{(2)}$ is desired, $L_y^0 L_y^0 L_z^0 \gg L_y^d L_y^d L_z^d$. Similarly, if our interest is in $\chi_d^{(2)}$ we look for a combination of angle and thickness for which $L_y^0 L_y^0 L_z^0 \ll L_y^d L_y^d L_z^d$. In cases where both interfaces are of interest, it is particularly intriguing to be able to prepare a film of thickness d and then locate two angles that achieve the desired interface selections. We start by considering the ratio of the results at $z = d$ to those at $z = 0$, as displayed in the right column of Fig. 4. Large values of this ratio display a selectivity for the second interface, after the beams have travelled through the film thickness d, with the actual path lengths determined by

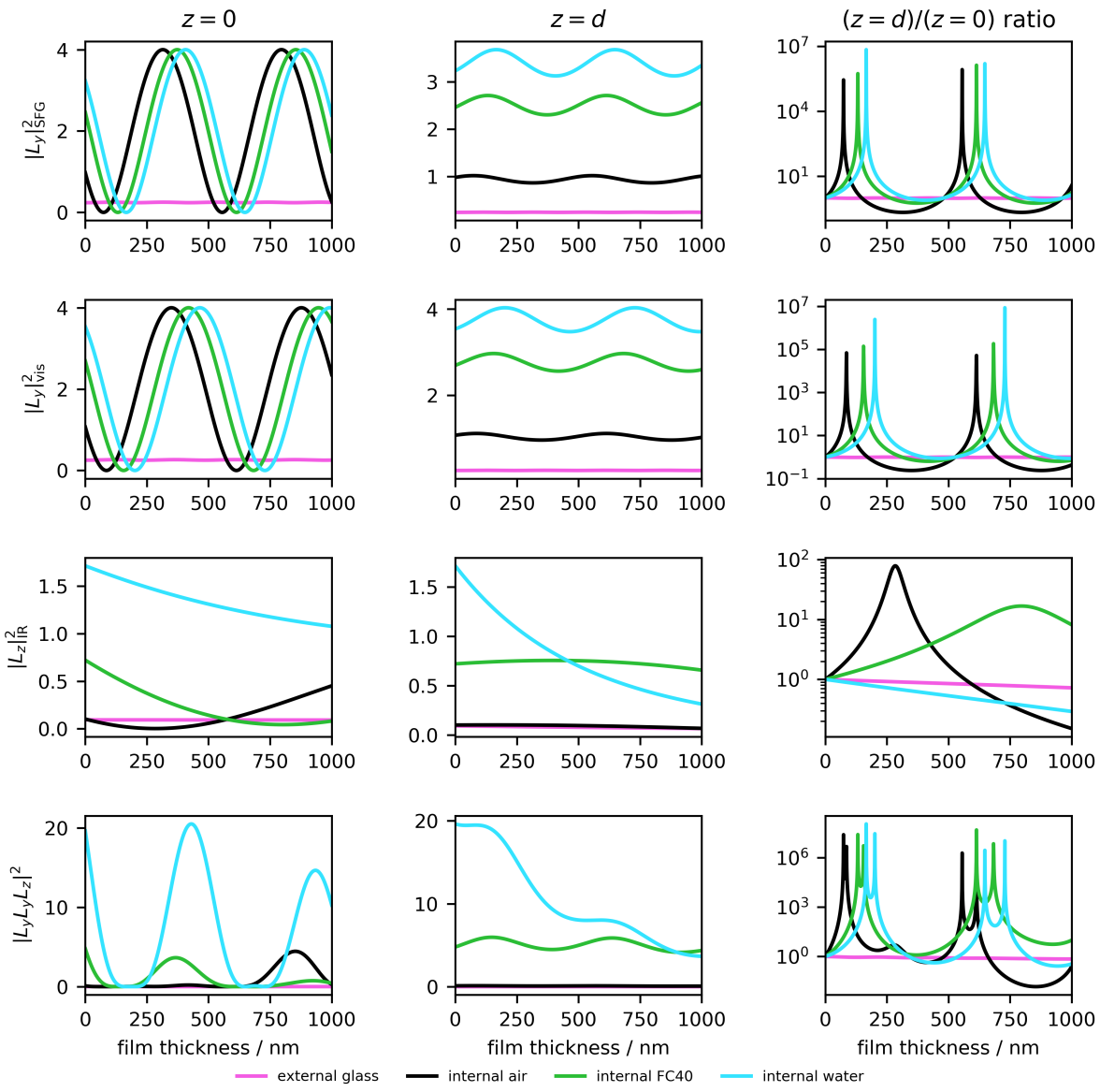

Figure 4: Mean square electric field amplitude, with respect to incident s- or p-polarized intensity at the first ($z = 0$, left column) and second ($z = d$, middle column) film interface for the SFG beam (top row), and incoming visible (second row) and infrared (third row) beams. The product of these three quantities, $|L_y L_y L_z|^2$, is plotted in the bottom row. In the right column, the ratio of each quantity at $z = d$ is plotted with respect to the corresponding values at $z = 0$ on a logarithmic scale. Results are illustrated for a PDMS film on glass (blue, $N_1 = 1$, beams incident from air), and internal reflection (N_1 corresponding to a silica prism), and N_3 corresponding to air (orange), water (red), and FC40 (green).

the angles of incidence. The bottom right panel is the figure of merit, the ratio of the squares of the products $|(LLL)_d/(LLL)_0|^2$. We have used a logarithmic scale is order to highlight very large and small values of this ratio, as both are of interest. A difficulty associated with such a graphical representation is that these figures apply to only a specific set of visible and IR beam angles. Since there is a limit to the accuracy to which film thickness can be determined, it would be more useful to see large values of this ratio that exist over a range of thickness.

A proposed solution is to generate selectivity maps as shown in Fig. 5. Here the individual values at $z = 0$ and $z = d$ are no longer shown, but the ratio is plotted directly, as a function of both angle of incidence and film thickness. The scaling challenge is addressed by coloring custom contour levels, regardless of the extent of the data. In our example, values of $|(LLL)_d/(LLL)_0|^2$ (or $|L^d/L^0|^2$ in the case of the individual beams) are red if they are greater than 100, and yellow for $10 < |(LLL)_d/(LLL)_0|^2 < 100$. Highlighting these custom contours simultaneously solves the reciprocal issue, as $|(LLL)_d/(LLL)_0|^2 < 0.01$ are dark blue and $0.001 < |(LLL)_d/(LLL)_0|^2 < 0.1$ are cyan. All other values ($0.1 < |(LLL)_d/(LLL)_0|^2 < 10$ are left white. In other words, white indicates that there is most likely insufficient selectivity of the two interfaces to make a distinction, and so that combination of thickness and angle is not useful.

A quick inspection of these results immediately reveals that external reflection geometries cannot, in general, be used to isolate contributions from a dielectric substrate–organic film vs film–air interface. For the internal reflection geometries, selectivity is possible, but only at angles above the critical angle. The rightmost column of Fig. 5 is the only required piece of information to make experimental decisions, but the relative contributions of the SFG, visible, and infrared beams may be used to understand the final results. There is no combination of film thickness or angle that achieves selectivity of the infrared field at any interface. However, the multiplicative selectivity of the SFG and visible beams is sufficient to create geometries that are selective for either interface. One additional feature has been incorporated into Fig. 5. Just because the ratio $|(LLL)_d/(LLL)_0|^2$ is large, doesn't mean that $|(LLL)_d|^2$ is of appreciable magnitude. In other words, it is not worth designing an experiment if the number of SFG counts will be below the noise level. We therefore

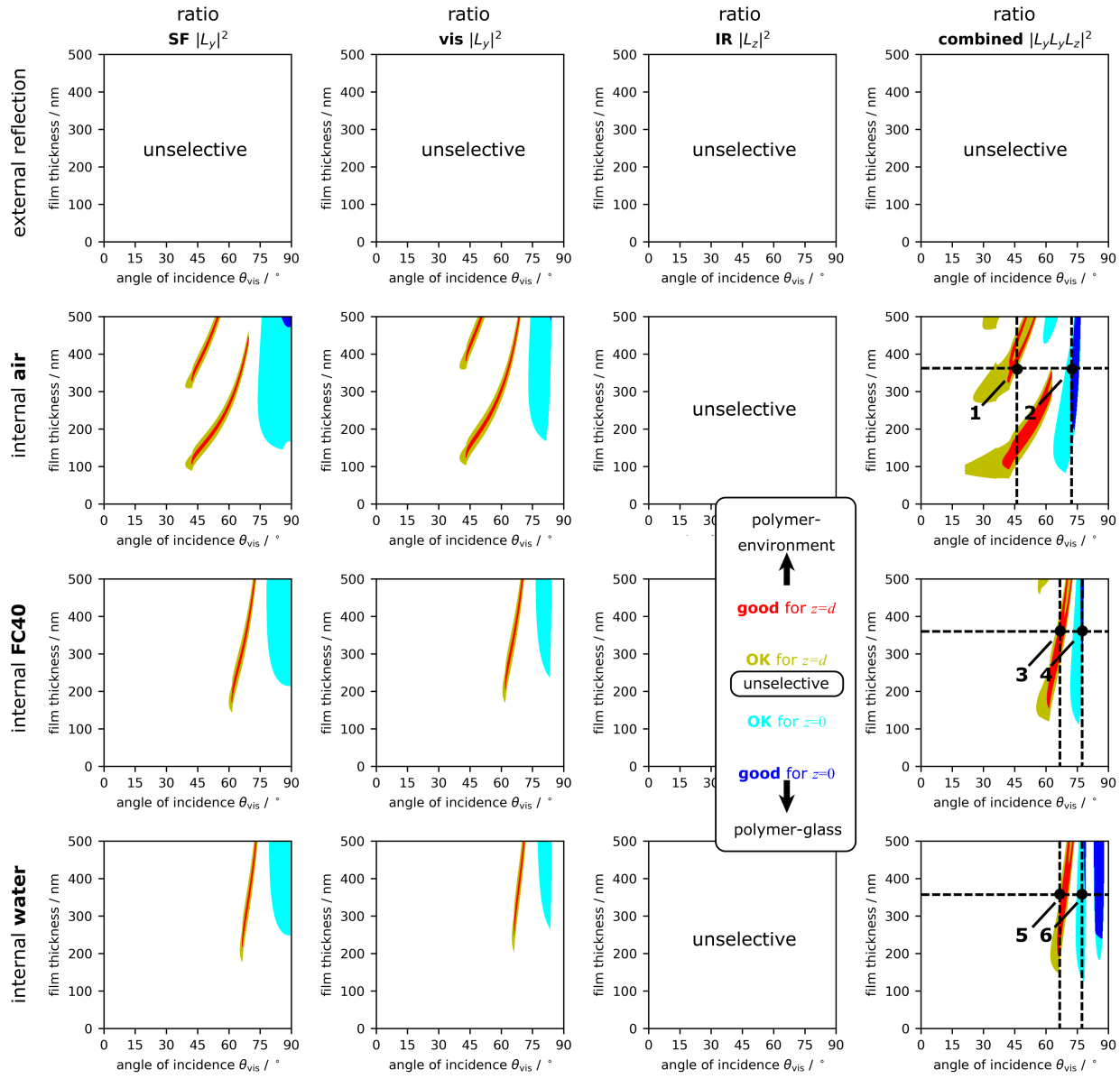

Figure 5: Ratio of the mean square fields L^d/L^0 as a function of film thickness and angle of incidence for the SFG beam (left column), visible (second column), infrared (third column), and product of the three factors ($|(LLL)_d/(LLL)_0|^2$, right column) for the case of external reflection (top row), and internal reflection with the environmental side of the PDMS being air (second row), FC40 (third row), or water (bottom row). Based on the local fields alone (i.e. no weighting from the relative $\chi^{(2)}$ contributions), white indicates insufficient selectivity for either interface. Values of thickness and angle that produce good selectivity ($|(LLL)_d/(LLL)_0|^2 > 10$) for the environmental side indicated in yellow; best selectivity ($|(LLL)_d/(LLL)_0|^2 > 100$) appear red. Likewise, good selectivity for the first interface ($|(LLL)_0/(LLL)_d|^2 > 10$) are in cyan; best sensitivity ($|(LLL)_0/(LLL)_d|^2 > 100$) are in dark blue.

incorporate one additional constraint in that $|(LLL)_d|^2$ must be greater than a threshold value, or else $|(LLL)_d/(LLL)_0|^2$ is colored white (instead of yellow or red). This value can be selected based on the sensitivity of the detector, of magnitude of the expected $\chi^{(2)}$ value. In this case, we have chosen unity. Likewise, cyan or blue is drawn only in the case where $|(LLL)_0|^2 > 1$.

Experimental Demonstration

We now use the above models to present results for PDMS spectra at the surface of fused silica, air, a perfluorinated liquid (FC40), and water. There are a total of six possible experiments that can be performed, as illustrated in Fig. 6. A typical workflow requires preparing a film close to the desired target thickness for the planned angle of incidence. For example, if we desire a film with a thickness of 400 nm, the crosshairs in Fig. 2a indicate that we should aim for a 6.5% wt/wt solution for casting at 5000 rpm. However, after this film was prepared, instead of the anticipated 56,000 counts of Raman for the 2905 cm^{-1} peak (dashed crosshairs in Fig. 2b), 50,680 counts were obtained (solid crosshairs), indicating that we have made a film with a thickness of 362 nm, and the corresponding angles of incidence are recalculated.

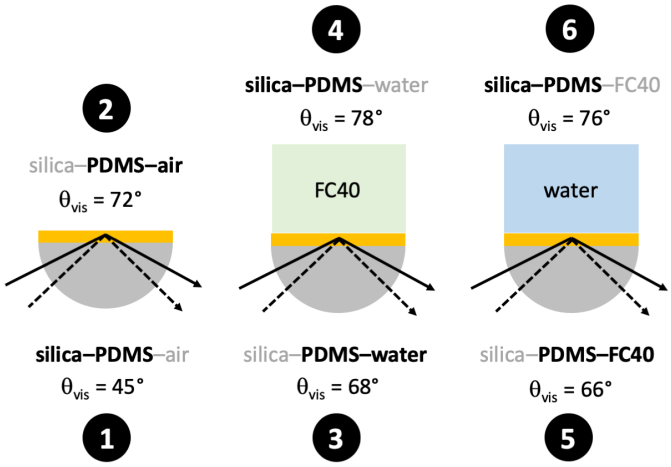

Figure 6: Six possible experiments that can be performed with PDMS on silica, adjacent to air, water, and FC40. In each case, $\theta_{\mathrm{IR}} = \theta_{\mathrm{vis}} + 9.8°$.

Now we simply need to vary the angle of incidence as depicted in Fig. 6 to selectively probe one of the two possible interfaces. Out of the six experiments performed with silica–PDMS–air,

silica–PDMS–FC40, and silica–PDMS–water, we anticipated that the data obtained from the three silica–PDMS interfaces ($z = 0$) should be similar, and this is demonstrated in Fig. 7a. On the other hand, when we probe the environmental sides we observed significantly different SFG spectra depending on the media it came in contact with. Two major peaks for PDMS are at 2910 cm^{-1} for the symmetric stretching and 2955 cm^{-1} for the antisymmetric stretching of the CH_3 group.[6,42–50] A mode near 2880 cm^{-1} has also been reported for the symmetric CH_2 stretch.[42,43,45–47] The ratio of the 2910 cm^{-1} and 2955 cm^{-1} modes has previously been observed to change depending on the hydrophobicity of the environment the CH_3 groups are interacting with, as PDMS has been shown to restructure when placed under water.[43,45,51] It has also been reported that 2910 cm^{-1} is the most intense mode when the environment is hydrophobic (air and FC40 in our case), whereas the intensity of the 2955 cm^{-1} is higher when the media is hydrophilic (water and glass in our case).[43,45,51] All the SFG spectra from the silica–PDMS interface obtained from the different experiments showed a predominant peak at 2955 cm^{-1} with a shoulder at 2910 cm^{-1} owing to the hydrophilicity of the silica. PDMS–water also produced a similar spectrum as shown in Fig. 7b. On the contrary, for hydrophobic media we observed a flipping of relative intensity of these two peaks. Although FC40 is considered to be ultra hydrophobic, we found that the CH_3 antisymmetric stretching intensity was higher than that observed at the PDMS–air interface. This points to a difference in molecular interaction that is also indicated by a 10 cm^{-1} spectral shift from 2950 cm^{-1} for FC40 to 2960 cm^{-1} for air.

These results are intriguing as, for a fixed film thickness, the prism–film interface ($z = 0$) can be probed with a given set of angles, the film–air interface ($z = d$) with another set of angles, and then an aqueous solution can be introduced to study the film restructuring (at $z = d$) simply by rotating to a third set of angles. If the solution conditions are varied in the experiment, a setup such as our motorized hemicylinder enables continuous monitoring of the film–solution interface as long as the refractive index of medium 3 is known or can be estimated.

A point of caution is that the formalism presented here assumes only dipolar contributions to $\chi^{(2)}$.[3,29] However, one cannot rule out the possibility of quadrupolar contributions to $\chi^{(2)}$,

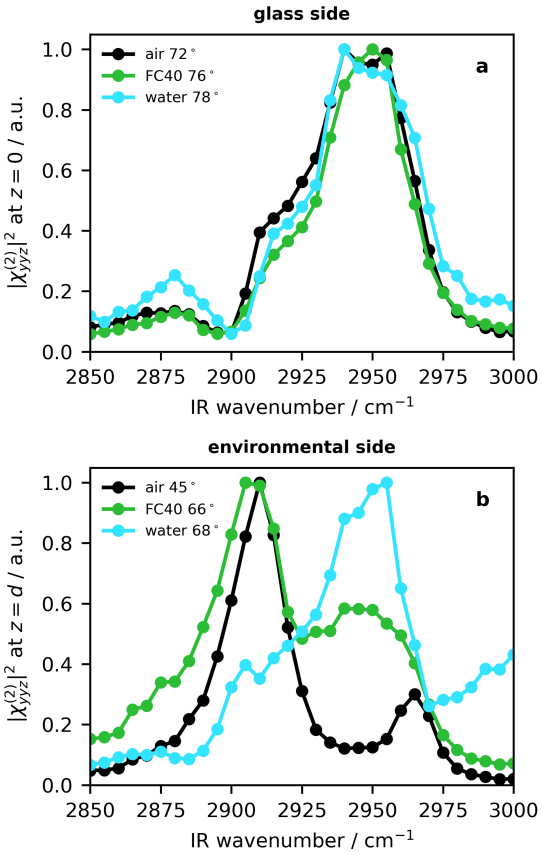

Figure 7: SFG spectra corresponding to the 6 different scenarios presented in Fig. 6 and identified in Fig. 5 for (a) the prism–film interface at $z = 0$ and (b) the film–air/FC40/water interfaces at $z = d$.

as has been demonstrated in several experiments.[52–58] Selectively probing the interface at $z = d$ necessitates the visible and infrared beams traversing the polymer film, so quadrupolar contributions may be significant. However, in cases where measurements of sufficiently thick films is possible in both internal and external reflection geometries, the spectra may be compared to those obtained for thin films.

Conclusions

We have provided explicit expressions for the commonly-encountered case of a film deposited on a substrate with SFG potentially originating at the first ($z = 0$) or second ($z = d$) interface. In the case

of external reflection (where the air–film interface is located at $z = 0$) there is no combination of thickness or angle that can selectively probe either interface when the film is coated on a dielectric substrate. However, the two interfaces can be selectively probed when using an internal reflection geometry. By plotting the ratio of the local field factors at $z = d$ to those at $z = 0$ using a logarithmic coloring scheme, suitable values of the film thickness and angles may be readily identified, even without any prior knowledge of the relative magnitude and phase of the $\chi^{(2)}$ contributions at either interface.

Acknowledgement

This work was supported by a Discovery Grant from the Natural Sciences and Engineering Research Council of Canada (NSERC), and an NSERC Collaborative Research and Discovery Grant in partnership with ASASoft (Canada) Inc. Equipment was purchased with support from the Canadian Foundation for Innovation and the British Columbia Knowledge Development Fund. Raman and profilometry measurements were performed at the University of Victoria Centre for Advanced Materials and Related Technologies (CAMTEC). Dr. Stanislav Konorov (UVic Chemistry) provided advice on the application of Raman spectroscopy to the thickness measurements. We thank Prof. Aaron Massari (University of Minnesota) and Prof. Sean Roberts (University of Texas at Austin) for stimulating discussions on the topic of multiple beam interference in SFG spectroscopy. We thank Prof. Akihiro Morita (Tohoku University) for valuable discussion on the topic of electric fields at interfaces.

References

(1) Shen, Y. R. *The Principles of Nonlinear Optics*; John Wiley & Sons: New York, 1984.

(2) Shen, Y. R. Surface Spectroscopy by Nonlinear Optics. Proc. Int. School of Physics, Ernico Fermi. Amsterdam, 1994; pp 139–165.

(3) Shen, Y. R. Basic Theory of Surface Sum-Frequency Generation. *J. Phys. Chem. C* **2012**, *116*, 15505–15509.

(4) Boyd, R. W. *Nonlinear Optics*, 2nd ed.; Academic Press: San Diego, 2003.

(5) Chen, Z.; Shen, Y. R.; Somorjai, G. A. Studies of Polymer Surfaces by Sum Frequency Generation Vibrational Spectroscopy. *Annu. Rev. Phys. Chem.* **2002**, *53*, 437–465.

(6) Chen, Z. Investigating Buried Polymer Interfaces Using Sum Frequency Generation Vibrational Spectroscopy. *Prog. Polym. Sci.* **2010**, *35*, 1376–1402.

(7) O'Brien, D.; Massari, A. Simulated Vibrational Sum Frequency Generation From a Multilayer Thin Film System With Two Active Interfaces. *J. Chem. Phys* **2013**, *138*, 154708.

(8) O'Brien, D. B.; Massari, A. M. Modeling Multilayer Thin Film Interference Effects in Interface-specific Coherent Nonlinear Optical Spectroscopies. *J. Opt. Soc. Am. B: Opt. Phys.* **2013**, *30*, 1503–1512.

(9) O'Brien, D. B.; Massari, A. M. Experimental Evidence For an Optical Interference Model for Vibrational Sum Frequency Generation on Multilayer Organic Thin Film Systems. I. Electric Dipole Approximation. *J. Chem. Phys.* **2015**, *142*, 024703.

(10) Lambert, A. G.; Neivandt, D. J.; Briggs, A. M.; Usadi, E. W.; Davies, P. B. Interference Effects in Sum Frequency Spectra from Monolayers on Composite Dielectric/Metal Substrates. *J. Phys. Chem. B* **2002**, *106*, 5461–5469.

(11) McGall, S. J.; Davies, P. B.; Neivandt, D. J. Interference Effects in Sum Frequencyy Vibrational Spectra of Thin Polymer Films: An Experimental and Modeling Investigation. *J. Phys. Chem. B* **2004**, *108*, 16030–16039.

(12) Tong, Y.; Zhao, Y.; Li, N.; Osawa, M.; Davies, P. B.; Ye, S. Interference Effects in the Sum Frequency Generation Spectra of Thin Organic Films. I. Theoretical Modeling and Simulation. *J. Chem. Phys* **2010**, *133*, 034704.

(13) Tong, Y.; Zhao, Y.; Li, N.; Ma, Y.; Osawa, M.; Davies, P. B.; Ye, S. Interference Effects in the Sum Frequency Generation Spectra of Thin Organic Films. II. Applications to Different Thin-film Sytems. *J. Chem. Phys* **2010**, *133*, 034705.

(14) Li, G.; Dhinojwala, A.; Yeganeh, M. S. Interference Effect from Buried Interfaces Investigated by Angular-Dependent Infrared–Visible Sum Frequency Generation Technique. *J. Phys. Chem. C* **2011**, *115*, 7554–7561.

(15) Moon, A. P.; Pandey, R.; Bender, J. A.; Cotton, D. E.; Renard, B. A.; Roberts, S. T. Using Heterodyne-Detected Electronic Sum Frequency Generation To Probe the Electronic Structure of Buried Interfaces. *J. Phys. Chem. C* **2017**, *121*, 18653–18664.

(16) Hirose, C.; Ishida, H.; Iwatsu, K.; Watanabe, N.; Kubota, J.; Wada, A.; Domen, K. In Situ SFG Spectroscopy of Film Growth. I. General Formulation And the Analysis of the Signal Observed During the Deposition of Formic Acid on Pt(110)-(1×2) Surface. *J. Chem. Phys.* **1998**, *108*, 5948–5956.

(17) Yeh, P. *Optical waves in layered media*; Wiley Online Library, 1988; Vol. 95.

(18) Sipe, J. New Green-function Formalism for Surface Optics. *J. Opt. Soc. Am. B: Opt. Phys.* **1987**, *4*, 481–489.

(19) Hankett, J. M.; Lu, X.; Liu, Y.; Seeley, E.; Chen, Z. Interfacial Molecular Restructuring of Plasticized Polymers in Water. *Phys. Chem. Chem. Phys.* **2014**, *16*, 20097–20106.

(20) Otsuki, Y.; Ishiyama, T. S. T.; Morita, A.; Watanabe, K.; Matsumoto, Y. Unveiling Subsurface Hydrogen-Bond Structure of Hexagonal Water Ice. *Phys. Rev. B* **2017**, *96*, 115405.

(21) Lu, X.; Clarke, M. L.; Li, D.; Wang, X.; Xue, G.; Chen, Z. A Sum Frequency Generation Vibrational Study of the Interference Effect in Poly(n-butyl methacrylate) Thin Films Sandwiched Between Silica and Water. *J. Phys. Chem. C* **2011**, *115*, 13759–13767.

(22) Backus, E. H. G.; Garcia-Araez, N.; Bonn, M.; Bakker, H. J. On the Role of Fresnel Factors in Sum-Frequency Generation Spectroscopy of Metal-Water and Metal-Oxide-Water Interfaces. *J. Chem. Phys. C* **2012**, *116*, 23351–23361.

(23) Wilk, D.; Johannsmann, D.; Stanners, C.; Shen, Y. Second-harmonic Generation from C_{60} Thin Films at 1.064 μm. *Phy. Rev. B* **1995**, *51*, 10057.

(24) Wang, J.; Paszti, Z.; Even, M. A.; Chen, Z. Interpretation of Sum Frequency Generation Vibrational Spectra of Interfacial Proteins by the Thin Film Model. *J. Phys. Chem. B* **2004**, *108*, 3625–3632.

(25) FitzGerald, W. R.; Jena, K. C.; Hore, D. K. Effects of Single-Source Multiple Beam Inteference in Vibrational Sum-Frequency Generation Spectroscopy. *J. Mol. Struct.* **2014**, *1084*, 368–373.

(26) Ramsay, M.; Beutier, C.; McGarvey, G. B.; Hore, D. K. Adsorption of Heptane-Toluene Binary Mixtures on a Hydrophobic Polymer Surface. *J. Chem. Phys.* **2019**, *150*, 014702.

(27) Koschwanez, J. H.; Carlson, R. H.; Meldrum, D. R. Thin PDMS Films Using Long Spin Times or Tert-Butyl Alcohol as a Solvent. *PLoS ONE* **2009**, *4(2)*, e4572.

(28) Braci, M.; Mohan, T.; Kargl, R.; Hribernik, T. G. S.; Kostler, S.; Stana-Kleinscheka, K.; Fras-Zemljic, L. Preparation of PDMS Ultrathin Films and Patterned Surface Modification with Cellulose. *RSC Adv.* **2014**, *4*, 11955–11961.

(29) Morita, A. *Theory of Sum Frequency Generation Spectroscopy*; Springer: Singapore, 2018.

(30) Born, M.; Wolf, E. *Principles of Optics*, 4th ed.; Pergamon Press Ltd.: Oxford, 1970.

(31) Hansen, W. N. Electric Fields Produced by the Propagation of Plane Coherent Electromagnetic Radiation in a Stratified Medium. *J. Opt. Soc. Am.* **1968**, *58*, 380–390.

(32) Axelsen, P. H.; Citra, M. J. Orientational Order Determination by Internal Reflection Infrared Spectroscopy. *Prog. Biophys. Molec. Biol.* **1996**, *66*, 227–253.

(33) Jena, K. C.; Hore, D. K. Variation of Ionic Strength Reveals the Interfacial Water Structure at a Charged Mineral Surface. *J. Phys. Chem. C* **2009**, *113*, 15364–15372.

(34) Zhuang, X.; Miranda, P. B.; Kim, D.; Shen, Y. R. Mapping Molecular Orientation and Conformation at Interfaces by Surface Nonlinear Optics. *Phys. Rev. B* **1999**, *59*, 12632–12640.

(35) Okuno, M.; Ishibashi, T.-a. Bulk-or-Interface Assignment of Heterodyne-Detected Chiral Vibrational Sum Frequency Generation Signal by its Polarization Dependence. *J. Chem. Phys.* **2018**, *149*, 244703.

(36) Wang, L.; Nihonyanagi, S.; Inoue, K.-i.; Nishikawa, K.; Morita, A.; Ye, S.; Tahara, T. Effect of Frequency-Dependent Fresnel Factor on the Vibrational Sum Frequency Generation Spectra for Liquid/Solid Interfaces. *J. Phys. Chem. C* **2019**, *123*, 15665–15673.

(37) Malitson, I. H. Interspecimen Comparison of the Refractive Index of Fused Silica. *J. Opt. Soc. Am.* **1965**, *55*, 1205–1209.

(38) Schneider, F.; Draheim, J.; Kamberger, R.; Wallrabe, U. Process and Material Properties of Polydimethylsiloxane (PDMS) for Optical MEMS. *Sens. Actuators, A* **2009**, *151*, 95–99.

(39) Querry, M. *Optical Constants of Minerals and Other Materials from the Millimeter to the Ultraviolet*; 1987.

(40) Segelstein, D. J. The Complex Refractive Index of Water. M.Sc. thesis, University of Missouri, Kansas City, 1981.

(41) 3M Electronics Markets Materials Division, *Product Information:Fluorinert™ Electronic Liquid FC-40*; 2010.

(42) Gragson, D. E.; McCarty, B. M.; Richmond, G. L. Ordering of Interfacial Water Molecules at the Charged Air/Water Interface Observed by Vibrational Sum Frequency Generation. *J. Am. Chem. Soc.* **1997**, *119*, 6144–6152.

(43) Zhang, D.; Ward, R.; Shen, Y.; Somorjai, G. Environment-Induced Surface Structural Changes of a Polymer: An in Situ IR + Visible Sum-Frequency Spectroscopic Study. *J. Phys. Chem. B* **1997**, *101*, 9060–9064.

(44) Chen, Z.; Ward, R.; Tian, Y.; Baldelli, S.; Opdahl, A.; Shen, Y.-R.; Somorjai, G. A. Detection of Hydrophobic End Groups on Polymer Surfaces by Sum-Frequency Generation Vibrational Spectroscopy. *J. Am. Chem. Soc.* **2000**, *122*, 10615–10620.

(45) Chen, C.; Wang, J.; Chen, Z. Surface Restructuring Behavior of Various Types of Poly(dimethylsiloxane) in Water Detected by SFG. *Langmuir* **2004**, *20*, 10186–10193.

(46) Ye, H.; Gu, Z.; Gracias, D. Kinetics of Ultraviolet and Plasma Surface Modification of Poly(dimethylsiloxane) Probed by Sum Frequency Vibrational Spectroscopy. *Langmuir* **2006**, *22*, 1863–1868.

(47) Ye, S.; McClelland, A.; Majumdar, P.; Stafslien, S. J.; Daniels, J.; Chisholm, B.; Chen, Z. Detection of Tethered Biocide Moiety Segregation to Silicone Surface Using Sum Frequency Generation Vibrational Spectroscopy. *Langmuir* **2008**, *24*, 9686–9694.

(48) Shi, Q.; Ye, S.; Spanninga, S. A.; Su, Y.; Jiang, Z.; Chen, Z. The Molecular Surface Conformation of Surface-tethered Polyelectrolytes on PDMS Surfaces. *Soft Matter* **2009**, *18*, 3487–3494.

(49) Kim, C.; Gurau, M. C.; Cremer, P. S.; Yu, H. Chain Conformation of Poly(dimethyl siloxane) at the Air/Water Interface by Sum Frequency Generation. *Langmuir* **2008**, *24*, 10155–10160.

(50) Hsiao, E.; Barnette, A. L.; Bradley, L. C.; Kim, S. H. Hydrophobic but Hygroscopic Polymer Films: Identifying Interfacial Species and Understanding Water Ingress Behavior. *ACS Appl. Mater. Interfaces* **2011**, *3*, 4236–4241.

(51) Hankett, J. M.; Liu, Y.; Zhang, X.; Zhang, C.; Chen, Z. Molecular Level Studies of Polymer

Behaviors at the Water Interface Using Sum Frequency Generation Vibrational Spectroscopy. *J. Poly. Sci.* **2013**, *51*, 311–328.

(52) Yamaguchi, S.; Shiratori, K.; Morita, A.; Tahara, T. Electric Quadrupole Contribution to the Nonresonant Background of Sum Frequency Generation at Air/Liquid Interfaces. *J. Chem. Phys.* **2011**, *134*, 184705.

(53) Sun, S.; Tian, C.; Shen, Y. R. Surface Sum-Frequency Vibrational Spectroscopy of Nonpolar Media. *Proc. Nat. Acad. Sci. USA* **2015**, *112*, 5883–5887.

(54) Held, H.; Lvovsky, A. I.; Wei, X.; Shen, Y. R. Bulk Contribution From Isotropic Media in Surface Sum-Frequency Generation. *Phys. Rev. B* **2002**, *66*, 205110.

(55) Maikhuri, D.; Rurohit, S. P.; Mathur, K. C. Quadrupole Second Harmonic Generation and Sum-Frequency Generation in ZnO Quantum Dots. *AIP Adv.* **2015**, *5*, 047115.

(56) Wei, X.; Hong, S.-C.; Lvovsky, A. I.; Held, H.; Shen, Y. R. Evaluation of Surface *vs* Bulk Contributions in Sum-Frequency Vibrational Spectroscopy Using Reflection and Transmission Geometries. *J. Phys. Chem. B* **2000**, *104*, 3349–3354.

(57) Matsuzaki, K.; Nihonyanagi, S.; Yamaguchi, S.; Nagata, T.; Tahara, T. Vibrational Sum Frequency Generation by the Quadrupolar Mechanism at the Nonpolar Benzene/Air Interface. *J. Phys. Chem. Lett.* **2013**, *4*, 1654–1658.

(58) Zheng, R.; Weo, W. M.; Shi, Q. Theoretical Investigation of Quadrupole Contribution to Surface Sum-Frequency Vibrational Spectroscopy. *Phys. Chem. Chem. Phys.* **2015**, *17*, 9068–9073.

Graphical TOC Entry